Available online at www.sciencedirect.com
SCIENCE DIRECT
Journal of Fluorine Chemistry 125 (2004) 1563–1578
JOURNAL OF FLUORINE CHEMISTRY
www.elsevier.com/locate/fluor

Energetics of hydride and electron pair attachment to $EX_3^{0/+}$ (E = B, C, Al, Si and X = F, Cl, Br, I) and the study of bonding trends among $EX_3^{0/+}$, $EX_3^{2-/-}$, and $EX_3H^{-/0}$ by use of ELF and NBO analyses

Hélène P.A. Mercier[a], Matthew D. Moran[a], Gary J. Schrobilgen[a,*], Reijo J. Suontamo[b,*]

[a]*Department of Chemistry, McMaster University, Hamilton, ON L8S 4M1, Canada*
[b]*Department of Chemistry, University of Jyväskylä, P.O. Box 35, FIN-40014 Jyväskylä, Finland*

Received 24 June 2004; received in revised form 5 August 2004; accepted 6 August 2004

This paper is dedicated to our friend and colleague Professor Ronald J. Gillespie on the occasion of his 80th birthday and in recognition of his many outstanding contributions across a broad spectrum of chemistry.

Abstract

A theoretical gas-phase ''ligand-free'' or ''electron pair affinity'' (EPA) approach, based on CCSD(T)/(SDB-)cc-pVTZ//MP2/(SDB-)cc-pVTZ electronic structure calculations, is introduced as a possible means for determining Lewis acidity trends among planar $EX_3^{0/+}$ (E = B, C, Al, Si; X = F, Cl, Br, I) species. In this treatment, the free electron pair is considered to be an extreme Lewis base. The calculated EPA values are compared with experimental Lewis acidities, previously calculated fluoride ion affinity (FIA) and hydride ion affinity (HA) trends, and are found to exhibit reasonable correlations in all cases. The bonding in the planar and trigonal pyramidal conformations of $EX_3^{0/+}$ and of the trigonal pyramidal Lewis base $EX_3^{2-/-}$ anions are assessed by use of natural bond orbital (NBO) and natural resonance theory (NRT) analyses. The NBO charges of the CX_3^+ (X = Cl, Br, I, $OTeF_5$) cations are shown to correlate with the cation–anion and cation–solvent contacts in the recently determined crystal structures of $[CCl_3][Sb(OTeF_5)_6]$, $[CBr_3][Sb(OTeF_5)_6]\cdot SO_2ClF$, $[CI_3][Al(OC(CF_3)_3)_4]$, and $[C(OTeF_5)_3][Sb(OTeF_5)_6]\cdot 3SO_2ClF$ and known fluoro-carbocation structures. Topological electron localization function (ELF) basin lobe isosurfaces and volumes are used to rationalize the Lewis acidity trends and bond ionicities of the $EX_3^{0/+}$ species, and Lewis basicities of the $EX_3^{2-/-}$ species.

Keywords: Trihalomethyl cations; Electronic structure calculations; Fluoride ion affinity; Electron pair affinity; Hydride ion affinity; Lewis acidity; Electron localization function (ELF)

1. Introduction

The recent application of fluorinated, weakly coordinating anions to the syntheses of salts of the trihalomethyl cations has made possible the isolation of examples of their salts, providing the crystal structures of $[CCl_3][Sb(OTeF_5)_6]$ [1], $[CBr_3][Sb(OTeF_5)_6]\cdot SO_2ClF$ [1], and $[CI_3][Al(OC(CF_3)_3)_4]$ [2] and the first determinations of the geometric parameters of the CX_3^+ (X = Cl, Br, I) cations. In addition, the structure of the $OTeF_5$ substituted carbocation, $C(OTeF_5)_3^+$, has recently been obtained from the crystal structure of $[C(OTeF_5)_3][Sb(OTeF_5)_6]\cdot 3SO_2ClF$ [1]. All four cations have local D_{3h} symmetries in their crystal structures.

Trihalomethyl cations, CX_3^+ (X = Cl, Br, I), have been the subject of considerable theoretical interest for some time. While solid-state structural data for trihalomethyl cations had been previously lacking, electronic structure calculations using various quantum mechanical methods had been used to predict the bonding and chemical properties for

* Corresponding authors. Tel.: +1 905 525 9140x23306; fax: +1 905 522 2509 (G.J. Schrobilgen); Tel.: +358 14 260 2605; fax: +358 14 260 2501 (R.J. Suontamo).
E-mail addresses: schrobil@mcmaster.ca (G.J. Schrobilgen), suontamo@cc.jyu.fi (R.J. Suontamo).

0022-1139/$ – see front matter © 2004 Elsevier B.V. All rights reserved.
doi:10.1016/j.jfluchem.2004.08.008

the isoelectronic CX_3^+ [1–13] and BX_3 [1,2,5,14–19] (X = F, Cl, Br, I) series and related isovalent species such as AH_2X^+ and YH_2X (X = F, Cl, Br, I; A = C, Si, Ge, Sn, Pb; Y = B, Al, Ga, In, Tl) [5]. Results abound for species where X = F [1,2,7,9–11,14–21] or Cl [1,2,6,7,12–19,21–23], but are relatively sparse for X = Br [1,2,4,6,7] and I [1,2,4,6]. The bonding and relative stabilities of the trihalomethyl cations have been assessed in terms of relative degrees of σ and π donation from the halogen atom to the carbon center [1,2,4,5,24–27]. The σ effect, from the perspective of the halogen atoms of CX_3^+, has been found to be strongly withdrawing in the case of fluorine and weakly donating in the case of chlorine, bromine, and iodine (I > Br > Cl). The π back-donation is correspondingly very weak for fluorine and stronger for the heavier halogens (I > Br > Cl > F), which runs counter to the bonding descriptions of the BX_3 series that are usually given in the current textbooks of inorganic chemistry [28–31].

The reaction enthalpy resulting from Lewis acid–base adduct formation has been explained in terms of geometrical changes [26] and the nature of the electron pair donor–acceptor bond [19,32]. While spectroscopic studies of the relative Lewis acidities of boron trihalide donor–acceptor adducts have been extensive [33,34], experimental thermodynamic data are sparse for BX_3 adducts [35–37] and nonexistent for CX_3^+ analogues. Gas-phase calorimetric measurements of TMA·BX_3 (TMA = trimethylamine) show that the interaction energy is 3.9 kcal mol^{-1} lower for BCl_3 than for BF_3 [37] and the heats of reaction for BX_3 (X = F, Cl, Br) with pyridine and nitromethane show that the bond strengths increase in the order $BF_3 < BCl_3 < BBr_3$ [35]. Photoelectron studies have shown that the donor–acceptor interaction is stronger in the TMA·BCl_3 and TMA·BBr_3 adducts than in the BF_3 adduct [36].

An extensive theoretical study of X_3Al–D donor–acceptor complexes (X = F, Cl, Br, I; D = YH_3, YX_3, X^-; Y = N, P, As) suggests that there is no simple correlation between the degree of charge transfer and the donor–acceptor bond dissociation energy [38]. However, taking into account all theoretical data relating to the stabilities of X_3Al–D systems, the dissociation energies were shown to follow the order F > Cl > Br > I [38]. A G2(MP2) study for X_3Al–NH_3 gives the same order for the complexation energies (F, −38.6 kcal mol^{-1}; Cl, −35.7 kcal mol^{-1}; Br, −33.8 kcal mol^{-1}), although the differences between energy values are quite small [39]. The calculated donor–acceptor bond energies are strongly dependent on the level of theory and basis set chosen because the basis set of each fragment is extended by the basis functions of the other fragment upon adduct formation. This effect augments the original basis set and is referred to as the "basis set superposition error" (BSSE) [40,41]. The BSSE may be taken into account by use of the counterpoise function [42], however, this method overestimates the value of the BSSE for strongly bound complexes. Often another bias, the so-called "basis set incompleteness error" (BSIE), which has a sign opposite to that of the BSSE, has a strong influence on the calculated bond energies. Occasionally, the BSSE and the BSIE fortuitously cancel each other so that unrealistic agreement between calculated and experimental bond energies is obtained [43].

Gas-phase fluoride ion affinities (FIA) [2,44,45], representing a hard base, and hydride ion affinities (HA) [5], representing a soft base, have also been used as indices of relative Lewis acidities. The FIA values have been previously calculated for all CX_3^+ and BX_3 (X = F, Cl, Br, I) species in the gas phase by the MP2/TZVPP method and in CH_2Cl_2 solution by use of the COSMO model [2]. The experimental order for the BX_3 series has been reproduced by FIA calculations, and for CX_3^+, the reverse order, $CF_3^+ > CCl_3^+ > CBr_3^+ > CI_3^+$, has been obtained. The calculated FIA values for AlF_3 (115.0 kcal mol^{-1}) and $AlCl_3$ (114.6 kcal mol^{-1}) indicate that AlF_3 is perhaps a marginally stronger Lewis acid than $AlCl_3$ and much stronger than BF_3 (83.1 kcal mol^{-1}) [45]. The experimental Al–N bond dissociation enthalpies for Cl_3Al–NH_3 (137.1 ± 5.9 kcal mol^{-1}) and Br_3Al–NH_3 (143.8 ± 4.6 kcal mol^{-1}) [38], indicate that $AlBr_3$ is a stronger Lewis acid than $AlCl_3$. Although no FIA values are available for the SiX_3^+ series, binding energies calculated for F_3Si^+–L (L = NH_3, OH_2, NCH) at the B3LYP/6-311G(2d,p) level indicate that SiF_3^+ is a much stronger Lewis acid than CF_3^+ [11]. It has been shown by tandem mass spectrometry [46] and by the gas-phase reaction of SiF_3^+ with Ng (Ng = Ar, Kr, Xe) in a selected ion flow tube (SIFT) apparatus [47] that SiF_3^+ forms the series of F_3SiNg^+ cations. Similar attempts to form the F_3CXe^+ cation in the gas phase were unsuccessful [47]. The gas-phase reaction of SiF_3^+ with NH_3 in a SIFT apparatus led to HF elimination instead of stable complex formation [48]. The Lewis acidity of $SiCl_3^+$ was demonstrated by tandem and multiple-stage mass spectrometry experiments using different substituted pyridines as the ligands which showed that $SiCl_3^+$·2(pyr$_1$ pyr$_2$) adducts formed [49].

In view of the foregoing discussion, there is a need for a Lewis acidity scale that is independent of the nature of the donor ligand and free of the BSSE error. In this study, the concept of electron pair affinities (EPA) of the Lewis acids $EX_3^{0/+}$ (E = B, C, Al, Si; X = F, Cl, Br, I) is introduced in order to devise a donor-independent approach to Lewis acidity and to compare trends with previously calculated FIA and HA values. The electron localization function (ELF) formalism is also explored as a means to correlate and visualize Lewis acidity trends.

2. Results and discussion

2.1. Modeled species, calculated geometric parameters and reactions

The geometries of $EX_3^{0/+}$ (D_{3h}), $EX_3^{2-/-}$ (C_{3v}) and $EX_3H^{-/0}$ (C_{3v}) (E = B, C, Al, Si; X = F, Cl, Br, I) were fully

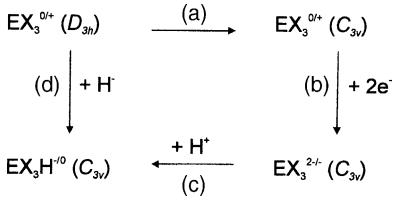

Scheme 1.

optimized at the MP2/(SDB-)cc-pVTZ level. The natural bond orbital (NBO) analyses, natural resonance analyses (NRT) and single point CCSD(T)/(SDB-)cc-pVTZ energy calculations were obtained for the optimized geometries. The optimized geometric and selected NBO parameters, namely, charges, valencies and ionic bond orders, are given in Table 1. All optimized structures were shown to be local minima by the fact that all vibrational frequencies were real. Calculated gas-phase reaction energies are given in Table 2 and an overview of the relevant reactions is provided in Scheme 1. A complete listing of calculated energies and NBO parameters can be found in the Supporting information.

In reaction (a) of Scheme 1, the optimized C_{3v} geometry of $EX_3^{2-/-}$ was used for $EX_3^{0/+}$ to obtain an estimate of the energy change that arises in going from the planar to the trigonal pyramidal structure (pyramidalization energy). As in previous studies [19,32], our estimate of the pyramidalization part of the total energy was obtained by a single point calculation in which the optimized pyramidal anion geometry is retained and the electron pair on E (E = B, C, Al, Si) is removed, as opposed to using constrained geometric parameters [50]. Reaction (b) of Scheme 1 describes the addition of a free electron pair to pyramidal $EX_3^{0/+}$ which can be viewed as a Lewis acid that is converted to a Lewis base and as a reduction half-equation. In step (c), $EX_3^{2-/-}$ behaves as a base by accepting a proton to form $EX_3H^{-/0}$ which can also be formed by hydride ion addition to the parent Lewis acid $EX_3^{0/+}$ according to reaction (d).

2.2. Geometries

All optimized geometries are in excellent agreement with available experimental [1,2,51] and previously calculated [5,38,49,51–55] values. The calculated E–X bond length is systematically longer in $EX_3^{2-/-}$ than in $EX_3^{0/+}$, and is consistent with the greater E–X bond polarity that is anticipated for an anion in which the E atom is in a lower formal oxidation state. Formal adduction of the lone pair of $EX_3^{2-/-}$ by H^+ leads to E–X bond lengths in $EX_3H^{-/0}$ that are intermediate with respect to those of $EX_3^{0/+}$ and $EX_3^{2-/-}$. For EX_3H^- (E = B, Al), the E–H bond lengths contract in the order F > Cl > Br > I, while the order is reversed in the SiX_3H series; the E–H bond lengths remain essentially constant in the CX_3H series.

2.3. Electron pair affinities and hydride ion affinities

The modeled electron pair affinities (EPA = $-\Delta E$ [kcal mol^{-1}]) derived from the combined reactions (a) + (b) (Table 2) are all negative for the BX_3 series in the order F (−196.5) < Cl (−104.6) < Br (−72.8) < I (−46.7) with BF_3 having the lowest EPA and representing the weakest Lewis acid in the BX_3 series. Thus, the calculated electron pair affinities follow the experimental Lewis acidity trend $BF_3 < BCl_3 < BBr_3 < BI_3$ [35] and the linear coefficient of determination, R^2, between FIA [2] and EPA values for BX_3 is excellent ($R^2 = 0.995$). The gas-phase electron pair affinities indicate that all four CX_3^+ species are stronger Lewis acids than their BX_3 analogues, and have a Lewis acidity trend [EPA, kcal mol^{-1}: F (228.8) > Br (226.4) > Cl (223.1) > I (221.6)] that is in reasonable agreement with, but does not linearly correlate with the FIA trends [kcal mol^{-1}: gas phase, F (263) > Cl (216) > Br (208) > I (194); CH_2Cl_2 solution, F (119) > Cl (85.8) > Br (82.0) > I (72.2)] [2]. The high Lewis acidity of CF_3^+ is consistent with its attendant high fluorophilicity and failed attempts to generate CF_3^+ in solution [4,56].

The electron pair affinities of the AlX_3 series exhibit a trend similar to that of the BX_3 series, with the overall EPA values being less negative in the order F (−101.5) < Cl (−50.1) < Br (−30.9) < I (−13.0). This trend is opposite to that calculated for the $X_3Al{\cdot}NH_3$ adducts [38,39,57] and the FIA values for AlF_3 and $AlCl_3$ [45], however, the experimental values for $Cl_3Al{\cdot}NH_3$ and $Br_3Al{\cdot}NH_3$ (vide supra) support the present EPA-based order. The EPA values for SiX_3^+ display the order F (253.3) > Cl (242.3) ≈ Br (242.2) > I (235.8) and are similar to those of the CX_3^+ series. The EPA of SiF_3^+ is larger than CF_3^+, and is corroborated by the calculated SiF_3^+–Lewis base binding energies [11] and the formation of the series of F_3SiNg^+ cations in the gas phase [42,43] and the inability to form F_3CXe^+ [47]. The results also indicate that their Lewis acidities are dominated by the pyramidalization energies (step (a)) in the case of the neutral EX_3 (E = B, Al) molecules, and by the energies of the electron pair attachments (reaction b), in the case of the isoelectronic EX_3^+ (E = C, Si) cations.

While the energy trends derived from reactions (a) and (b), when taken alone, are irregular, their sums, corresponding to the EPA values, show regular trends and agree with known and previously calculated Lewis acidity trends. For reaction (c), proton affinities of the $EX_3^{2-/-}$ anions can be taken as measures of gas-phase basicities. For all $EX_3^{2-/-}$ (E = B, C, Al, Si; X = F, Cl, Br, I), the values are highly exothermic (Table 2), and the trend is F > Cl > Br > I for the basicities within each series. The fact that all EX_3^{2-} (E = B, Al) anions are stronger Lewis bases than the EX_3^- (E = C, Si) anions can be rationalized in terms of their greater negative charges.

The hydride ion affinities derived from reaction (d) are all exothermic, and, as expected, follow the same trends as the EPA values, with R^2-values of 0.953 (B), 0.704 (C), 0.974

Table 1
NBO natural charges, natural valencies, geometric parameters, ionic contributions to the natural bond orders[a] and total bond energies for $EX_3^{0/+}$, $EX_3^{2-/-}$, and $EX_3H^{-/0}$ (E = B, C, Al, Si and X = F, Cl, Br, I)

E = C [Si]	Atom	Charge	Valency	Bond length (Å) and ∠ bond angle (°)		Ionic bond order	Total bond energy[b] (kcal mol^{-1})
EF_3^+ (D_{3h})	E	1.369 [2.656]	4.000 [3.941]	E–F_i	1.233 [1.529]	0.695 [1.031]	388.3 [365.5]
	F_i	−0.123 [−0.552]	1.333 [1.314]				
EF_3^- (C_{3v})	E	0.441 [1.164]	3.115 [3.752]	E–F_i	1.429 [1.682]	0.644 [1.078]	
	F_i	−0.480 [−0.721]	1.039 [1.251]	∠(F_i–E–F_j)	99.6 [96.5]		
EF_3^+ (C_{3v})	E	1.360 [2.463]	3.797 [3.733]	E–F_i	1.429 [1.682]	0.635 [0.922]	
	F_i	−0.120 [−0.488]	1.266 [1.244]	∠(F_i–E–F_j)	99.6 [96.5]		
EF_3H (C_{3v})	E	0.905 [2.198]	3.977 [3.917]	E–F_i	1.333 [1.583]	0.478 [0.761]	
	F_i	−0.333 [−0.630]	1.008 [0.993]	E–H	1.085 [1.453]	0.114 [0.295]	
	H	0.093 [−0.308]	0.952 [0.939]	∠(F_i–E–F_j)	108.6 [108.3]		
				∠(F_i–E–H)	110.4 [110.6]		
ECl_3^+ (D_{3h})	E	−0.091 [1.513]	3.938 [3.907]	E–Cl_i	1.645 [1.956]	0.293 [0.737]	303.0 [265.0]
	Cl_i	0.364 [−0.171]	1.313 [1.302]				
ECl_3^- (C_{3v})	E	−0.318 [0.693]	2.974 [3.403]	E–Cl_i	1.881 [2.201]	0.366 [0.829]	
	Cl_i	−0.227 [−0.564]	0.991 [1.134]	∠(Cl_i–E–Cl_j)	102.8 [97.4]		
ECl_3^+ (C_{3v})	E	0.095 [1.422]	3.784 [3.322]	E–Cl_i	1.881 [2.201]	0.289 [0.595]	
	Cl_i	0.302 [−0.141]	1.261 [1.107]	∠(Cl_i–E–Cl_j)	102.8 [97.4]		
ECl_3H (C_{3v})	E	−0.227 [1.286]	3.913 [3.899]	E–Cl_i	1.764 [2.037]	0.131 [0.537]	
	Cl_i	0.010 [−0.359]	0.986 [0.993]	E–H	1.081 [1.462]	0.221 [0.176]	
	H	0.196 [−0.210]	0.956 [0.920]	∠(Cl_i–E–Cl_j)	111.0 [109.5]		
				∠(Cl_i–E–H)	107.9 [109.5]		
EBr_3^+ (D_{3h})	E	−0.451 [1.121]	3.919 [3.887]	E–Br_i	1.801 [2.113]	0.343 [0.641]	277.7 [236.1]
	Br_i	0.484 [−0.040]	1.306 [1.296]				
EBr_3^- (C_{3v})	E	−0.512 [0.516]	3.027 [3.305]	E–Br_i	2.044 [2.374]	0.311 [0.744]	
	Br_i	−0.162 [−0.505]	1.009 [1.102]	∠(Br_i–E–Br_j)	103.4 [98.0]		
EBr_3^+ (C_{3v})	E	−0.552 [1.058]	2.696 [3.262]	E–Br_i	2.044 [2.374]	0.418 [0.501]	
	Br_i	0.517 [−0.019]	0.899 [1.087]	∠(Br_i–E–Br_j)	103.4 [98.0]		
EBr_3H (C_{3v})	E	−0.483 [0.995]	3.894 [3.881]	E–Br_i	1.918 [2.197]	0.085 [0.459]	
	Br_i	0.096 [−0.266]	0.979 [0.989]	E–H	1.081 [1.464]	0.219 [0.158]	
	H	0.194 [−0.197]	0.958 [0.915]	∠(Br_i–E–Br_j)	111.6 [109.9]		
				∠(Br_i–E–H)	107.2 [109.1]		
EI_3^+ (D_{3h})	E	−1.031 [0.502]	3.903 [3.850]	E–I_i	2.021 [2.345]	0.485 [0.473]	249.9 [200.8]
	I_i	0.677 [0.166]	1.301 [1.283]				
EI_3^- (C_{3v})	E	−0.833 [0.192]	2.962 [3.186]	E–I_i	2.267 [2.613]	0.187 [0.608]	
	I_i	−0.056 [−0.397]	0.987 [1.062]	∠(I_i–E–I_j)	105.2 [99.3]		
EI_3^+ (C_{3v})	E	−0.899 [0.541]	2.864 [3.221]	E–I_i	2.267 [2.613]	0.401 [0.386]	
	I_i	0.633 [0.153]	0.955 [1.074]	∠(I_i–E–I_j)	105.2 [99.3]		
EI_3H (C_{3v})	E	−0.893 [0.529]	3.881 [3.866]	E–I_i	2.139 [2.432]	0.228 [0.319]	
	I_i	0.237 [−0.114]	0.974 [0.985]	E–H	1.082 [1.470]	0.209 [0.139]	
	H	0.183 [−0.187]	0.959 [0.912]	∠(I_i–E–I_j)	112.6 [110.6]		
				∠(I_i–E–H)	106.1 [108.4]		

E = B [Al]	Atom	Charge	Valency	Bond length (Å) and ∠ bond angle (°)		Ionic bond order	Total bond energy[b] (kcal mol^{-1})
EF_3 (D_{3h})	E	1.392 [2.180]	4.000 [3.955]	E–F_i	1.315 [1.647]	0.957 [1.151]	459.2 [408.8]
	F_i	−0.464 [−0.727]	1.333 [1.318]				
EF_3^{2-} (C_{3v})	E	0.030 [0.459]	3.428 [3.860]	E–F_i	1.531 [1.815]	0.924 [1.187]	
	F_i	−0.677 [−0.820]	1.143 [1.287]	∠(F_i–E–F_j)	98.6 [97.3]		
EF_3 (C_{3v})	E	1.438 [2.094]	3.876 [3.860]	E–F_i 1.531 [1.815]	0.923 [1.098]		
	F_i	−0.479 [−0.698]	1.292 [1.287]	∠(F_i–E–F_j)	98.6 [97.3]		
EF_3H^- (C_{3v})	E	0.992 [1.841]	3.979 [3.934]	E–F_i	1.418 [1.713]	0.697 [0.851]	
	F_i	−0.567 [−0.759]	1.009 [0.994]	E–H	1.232 [1.613]	0.265 [0.551]	
	H	−0.291 [−0.565]	0.951 [0.951]	∠(F_i–E–H)	108.6 [108.6]		
				∠(F_i–E–H)	110.3 [110.3]		
ECl_3 (D_{3h})	E	0.335 [1.501]	3.953 [3.897]	E–Cl_i	1.740 [2.081]	0.650 [0.955]	310.7 [295.7]
	Cl_i	−0.112 [−0.500]	1.318 [1.299]				
ECl_3^{2-} (C_{3v})	E	−0.128 [0.350]	3.263 [3.540]	E–Cl_i	2.157 [2.453]	0.814 [1.042]	
	Cl_i	−0.624 [−0.783]	1.088 [1.180]	∠(Cl_i–E–Cl_j)	98.4 [96.0]		
ECl_3 (C_{3v})	E	0.661 [1.484]	3.726 [3.445]	E–Cl_i	2.157 [2.453]	0.678 [0.842]	
	Cl_i	−0.220 [−0.495]	1.242 [1.148]	∠(Cl_i–E–Cl_j)	98.4 [96.0]		

Table 1 (*Continued*)

E = B [Al]	Atom	Charge	Valency	Bond length (Å) and ∠ bond angle (°)		Ionic bond order	Total bond energy[b] (kcal mol^{-1})
$ECl_3H^-(C_{3v})$	E	0.126 [1.282]	3.937 [3.904]	E–Cl_i	1.878 [2.187]	0.457 [0.716]	
	Cl_i	−0.339 [−0.612]	0.993 [0.988]	E–H	1.194 [1.590]	0.086 [0.426]	
	H	−0.108 [−0.446]	0.958 [0.940]	∠(Cl_i–E–Cl_j)	109.6 [108.3]		
				∠(Cl_i–E–H)	109.4 [110.6]		
EBr_3 (D_{3h})	E	0.063 [1.263]	3.941 [3.858]	E–Br_i	1.891 [2.232]	0.583 [0.893]	269.5 [260.9]
	Br_i	−0.021 [−0.421]	1.314 [1.286]				
EBr_3^{2-} (C_{3v})	E	−0.148 [0.359]	3.177 [3.438]	E–Br_i	2.367 [2.726]	0.774 [1.005]	
	Br_i	−0.617 [−0.786]	1.059 [1.146]	∠(Br_i–E–Br_j)	99.7 [94.0]		
EBr_3 (C_{3v})	E	0.405 [1.218]	3.598 [3.185]	E-Br_i	2.367 [2.726]	0.589 [0.719]	
	Br_i	−0.135 [−0.406]	1.199 [1.062]	∠(Br_i–E–Br_j)	99.7 [94.0]		
EBr_3H^- (C_{3v})	E	−0.066 [1.112]	3.923 [3.893]	E–Br_i	2.031 [2.346]	0.401 [0.677]	
	Br(*i*)	−0.279 [−0.562]	0.988 [0.986]	E–H	1.188 [1.586]	0.073 [0.406]	
	H	−0.096 [−0.428]	0.959 [0.935]	∠(Br_i–E–Br_j)	110.0 [108.4]		
				∠(Br_i–E–H)	108.9 [110.6]		
EI_3 (D_{3h})	E	−0.428 [0.848]	3.925 [3.812]	E–I_i	2.116 [2.460]	0.448 [0.789]	217.3 [213.1]
	I_i	0.143 [−0.283]	1.308 [1.271]				
EI_3^{2-} (C_{3v})	E	−0.359 [0.193]	3.162 [3.342]	E–I_i	2.621 [2.971]	0.704 [0.930]	
	I_i	−0.547 [−0.731]	1.054 [1.114]	∠(I_i–E–I_j)	102.6 [99.4]		
EI_3 (C_{3v})	E	0.005 [0.852]	3.550 [3.207]	E–I_i	2.621 [2.971]	0.474 [0.650]	
	I_i	−0.002 [−0.284]	1.183 [1.069]	∠(I_i–E–I_j)	102.6 [99.4]		
EI_3H^- (C_{3v})	E	−0.397 [0.805]	3.894 [3.875]	E–I_i	2.255 [2.582]	0.291 [0.599]	
	I_i	−0.164 [−0.463]	0.981 [0.983]	E–H	1.186 [1.584]	0.084 [0.388]	
	H	−0.110 [−0.417]	0.951 [0.927]	∠(I_i–E–I_j)	110.9 [108.6]		
				∠(I_i–E–H)	108.3 [110.3]		

[a] Computations were carried out at the MP2/(SDB-)cc-pVTZ level.
[b] Total bond energies (gas-phase atomization energies) calculated at the CCSD(T)/(SDB-)cc-pVTZ//MP2/(SDB-)cc-pVTZ level.

(Al), and 0.972 (Si). The poor correlation for CX_3^+ arises from the reversed EPA order for X = Cl and Br. The HA values also exhibit trends similar to those calculated for the relative hydride ion affinities of EX_3 (E = B, Al) determined from the isodesmic reactions of EX_3 with EH_4^- [5].

2.4. Natural charges and valencies

Several methods have been used to apportion the calculated total electron density among bonded atoms in molecules [19,58]. These approaches usually overestimate charges by over-localizing the electron pair into a particular region of space. Thus, atomic charges cannot be directly used to rationalize relative Lewis acidities. Moreover, atomic charges can neither be observed experimentally, because they do not correspond to any unique physical property, nor can they be accurately calculated, because there is no quantum chemical operator that can produce an exact atomic charge eigenvalue for an atom in a molecule. Thus, electron-partitioning schemes are inherently arbitrary, and their reliability in defining the charge of an atom in a molecule is not guaranteed with respect to the use of different basis sets and levels of theory. Calculated atomic charges have, however, proven to be a useful concept in describing various chemical properties in at least a semi-quantitative way.

The relative advantages and disadvantages of methods developed for the calculation of atomic charges have been discussed in the standard textbooks [40,41,59]. Mulliken population analyses [60] do not produce charges that converge when the basis sets are enlarged [40]. Natural charges from natural bond orbital analysis (NBO) [61] show less basis set dependence and better convergence [40]. In addition, natural charges follow trends in electronegativity differences between bonded atoms [62]. When studying molecular interactions, charges calculated from electrostatic potential (ESP) fitting are recommended [59]. It must, however, be understood that there is a serious danger of over-interpretation by placing too much significance on the numerical value of a calculated atomic charge. As in the present study, NBO natural charges can be used to discuss *trends* in bonding when large basis sets (e.g., split valence triple zeta correlation consistent basis sets with d- and f-polarization functions, cc-pVTZ) are used in conjunction with electron correlation methods (e.g., MP2) [40].

Natural charges derived from natural orbital analyses [61] are given in Table 1. The charges on the central E atom become more negative, in a near-linear fashion, with the electronegativity difference, $\Delta\chi$(E–X), indicating considerable charge transfer for X = Cl, Br, and I. Such charge transfers have been previously discussed in terms of relative σ- and π-electron donor contributions from the halogen atom to the central boron or carbon atom in references [1,2,5,21,25–27,59]. For the reasons mentioned earlier, bonding discussions in the present context are restricted to natural valencies for the E and X atoms and natural ionic bond orders for E–X and E–H bonds (Table 1) calculated by

Table 2
Calculated[a] gas-phase reaction energies (kcal mol^{-1})[b]

	F	Cl	Br	I
(a) Pyramidalization energy: $EX_3^{0/+}$ (D_{3h}) → $EX_3^{0/+}$ (C_{3v})				
B	124.1	128.8	119.1	96.0
C	134.7	89.4	126.2	88.9
Al	74.8	92.5	104.2	80.6
Si	90.6	80.4	69.9	54.8
(b) Electron attachment energy: $EX_3^{0/+}$ (C_{3v}) + 2e$^-$ → $EX_3^{2-/-}$ (C_{3v})				
B	72.4	−24.2	−46.3	−50.2
C	−363.5	−312.5	−352.6	−310.5
Al	26.7	−42.4	−73.3	−67.6
Si	−343.9	−322.7	−312.1	−290.6
(a) + (b) ΔE = −EPA: $EX_3^{0/+}$ (D_{3h}) + 2e$^-$ → $EX_3^{2-/-}$ (C_{3v})				
B	196.5	104.6	72.8	45.7
C	−228.8	−223.1	−226.4	−221.6
Al	101.5	50.1	30.9	13.0
Si	−253.3	−242.3	−242.2	−235.8
(c) Proton affinity: $EX_3^{2-/-}$ + H$^+$ → $EX_3H^{-/0}$ (C_{3v})				
B	−594.7	−529.3	−506.5	−486.2
C	−399.8	−372.8	−364.6	−359.7
Al	−526.5	−483.0	−466.4	−449.2
Si	−371.4	−346.0	−336.8	−329.7
(d) Hydride ion affinity (HA): $EX_3^{0/+}$ (D_{3h}) + H$^-$ → $EX_3H^{-/0}$ (C_{3v})				
B	−86.8	−113.2	−122.3	−129.1
C	−317.2	−284.5	−279.6	−269.8
Al	−113.5	−121.4	−124.0	−124.7
Si	−313.2	−276.9	−267.5	−254.1

[a] Computations were carried out at the CCSD(T)/(SDB-)cc-pVTZ//MP2/(SDB-)cc-pVTZ level.
[b] Labels (a)–(d) refer to the gas-phase transformations given in Scheme 1.

means of the natural resonance theory [63] using 11 natural NBO Lewis reference structures. The natural valencies on atom E in $EX_3^{0/+}$ (D_{3h}) are close to four while the X atom valencies are between 1.27 and 1.33. The dominant natural Lewis resonance structure is that corresponding to three formal σ bonds and one formal π bond. The ionic (electrovalent) part of the natural E–X bond order systematically follows the natural charge differences of E and X (Table 1). The total bonding (gas-phase atomization) energy of $EX_3^{0/+}$ (D_{3h}) is largest for X = F and decreases with the ionic part of natural bond order over the series F > Cl > Br > I. Thus, the bonding is mainly ionic in $EF_3^{0/+}$ and is responsible for the high E–F bond energies. When going down the series of heavier halogens, the ionic character decreases and covalent character increases leading to lower bond energies (Table 1). These results are in accord with the ligand close packing (LCP) bonding model presented by Gillespie and co-workers [27] which espouses highly ionic characters for the E–X bonds of BF_3, BCl_3, and CF_3^+ as well as for BF_4^-, BCl_4^-, and CF_4.

The geometry change in step (a) leads to a decrease in the E valency, which still remains high (>3.1). In the resulting natural Lewis structures, the three original σ-bonds with high electron populations remain, but the one π bond is replaced by a formally anti-bonding lone pair (LP*) located on E having low electron populations (0.11–0.77 e). The E valency is further reduced in reaction (b), but remains, for the most part, greater than 3. The resulting $EX_3^{2-/-}$ anions have three σ-bonds and the original π-bond electron population is assigned to a lone pair (LP) on the E atom according to the NBO analyses.

2.4.1. Calculated charges and their correlations with solid-state structures

In the X-ray crystal structures of $[CCl_3][Sb(OTeF_5)_6]$ and $[CBr_3][Sb(OTeF_5)_6]\cdot SO_2ClF$ [1], the chlorine and bromine atoms of the CCl_3^+ and CBr_3^+ cations interact with the fluorine atoms of the anion and, in the case of the CBr_3^+ salt, with the oxygen atoms of SO_2ClF as shown in Fig. 1a and b. These interactions are shorter than or are at the limits of the sums of the accepted halogen–fluorine (oxygen) van der Waals radii (Cl···F, 3.15 Å [64], 3.22 Å [65]; Br···O, 3.35 Å [64], 3.37 Å [65]; Br···F, 3.30 Å [64], 3.32 Å [65]; I···F, 3.50 Å [64], 3.45 Å [65]) and are consistent with the positive charges that have been allocated to the halogen atoms of these cations in this and prior computational studies. The I···F contacts in $[CI_3][Al(OC(CF_3)_3)_4]$ [2] range from 3.29 to 3.58 Å and suggest less cation–anion interaction through the halogen ligands despite the net positive charges allocated to the iodine atoms which may, in part, be a consequence of the diffuse nature of the positive charges on the larger iodine ligands.

The $Sb(OTeF_5)_6^-$ salts also exhibit long contacts between the carbon atoms of CCl_3^+ (2.962(9)–3.574(11) Å) and CBr_3^+ (3.09(2), 3.39(2) Å) [1] and the fluorine atoms of the anions which are at the limit of or longer than the sum of the C···F van der Waals radii (3.10 [64], 3.30 [65]). The C···F contacts of these structures are comparable to those observed in $[CI_3][Al(OC(CF_3)_3)_4]$ [2] (3.26, 3.69, 3.76 Å) and are consistent with the negative charges that have been allocated to the carbon centers of all three trihalomethyl cations (Table 1). With the exception of the shortest C···F contact distance in $[CI_3][Al(OC(CF_3)_3)_4]$, no other C···F contacts approach the carbocation center of CI_3^+ along the pseudo-three-fold axis of its vacant p-orbital.

The coordination behaviors of the CX_3^+ (X = Cl, Br, I) cations in their presently known salts are in marked contrast with the C···F contact distances and contact angles in $[(m\text{-}CF_3C_6H_4)(C_6H_5)CF][As_2F_{11}]$ (3.01(2), 3.07(2) Å), $[(m\text{-}CF_3C_6H_4)(C_6H_5)CF][AsF_6]$ (2.78(1), 2.79(1) Å), and $[(CH_3)_2CF][AsF_6]$ (2.66(1), 2.78(1) Å) [21]. All three salts exhibit carbocation environments in which the trigonal planar cation interacts with fluorine ligands of neighboring AsF_6^- or $As_2F_{11}^-$ anions along the trajectory of the vacant p-orbital of carbon to give trigonal bipyramidal coordination at the carbocation center. Moreover, the C···F contact distances are significantly shorter than the accepted values for the sums of the van der Waals radii. The study notes that the coordination behaviors of these monofluorinated carbocations are consistent with positive charges at the carbocation center. The calculated positive natural charge on the trigonal planar carbon was confirmed, and was found to be 0.922 in the present work for $(CH_3)_2CF^+$ at the MP2/cc-

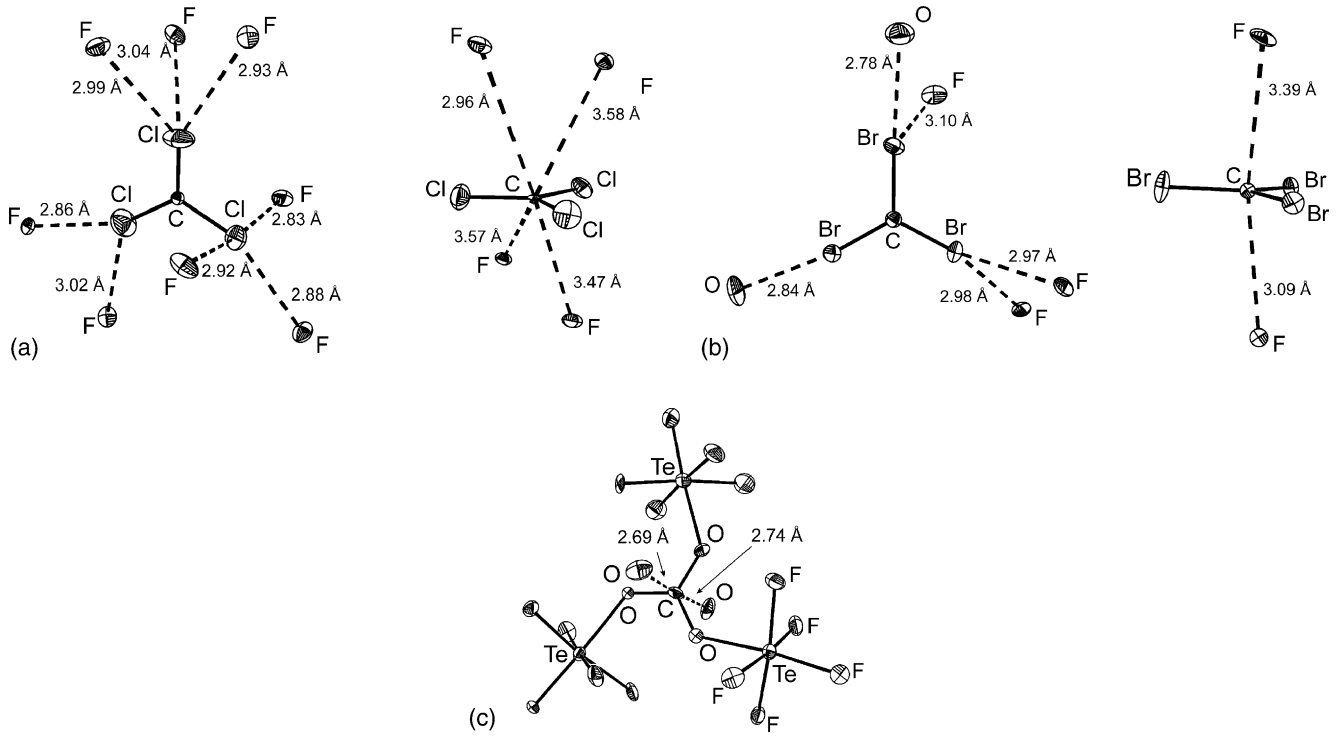

Fig. 1. Diagrams showing the halogen–fluorine/oxygen and carbon-fluorine/oxygen contacts for the X-ray crystal structures of (a) CCl_3^+ in $[CCl_3][Sb(OTeF_5)_6]$, (b) CBr_3^+ in $[CBr_3][Sb(OTeF_5)_6]\cdot SO_2ClF$, and (c) $C(OTeF_5)_3^+$ in $[C(OTeF_5)_3][Sb(OTeF_5)_6]\cdot 3SO_2ClF$.

pVTZ level of theory (see Section 4), which also provided geometric parameters that are in good agreement with those of the experimental structure.[1]

The coordination behaviors of the CX_3^+ (X = Cl, Br, I) cations also contrast with that of the $C(OTeF_5)_3^+$ cation in the crystal structure of $[C(OTeF_5)_3][Sb(OTeF_5)_6]\cdot 3SO_2ClF$ [1] (Fig. 1c). In this instance, the carbon atom is coordinated to the two oxygen ligands of two SO_2ClF molecules which again results in trigonal bipyramidal coordination around the central carbon atom, and C···O contacts (2.69(2), 2.74(2) Å) that are significantly less than the van der Waals radii sums for the oxygen and carbon atoms (3.15 [64], 3.20 [65]). The C···O contact distances and coordination around carbon are again consistent with the calculated positive charge on carbon (1.30) at the HF/SDB-cc-pVTZ level of theory. Moreover, this charge is similar to those predicted for CF_3^+ (1.57), BF_3 (1.56) and $B(OTeF_5)_3$ (1.45) at the same level of theory [1]. It is worth noting that the homologous series of $H_{3-n}C(ChH)_n^+$ (Ch = O, S, Se, Te) cations has been investigated by quantum mechanical calculations (natural population analysis calculations at the MP2(full)/LANL1DZ + P′ level) [66]. The carbon atom is positively charged for $C(OH)_3^+$ (1.212), whereas the charges on carbon for the remaining members of the series are negative, with the negative charge increasing upon descending group 16. This trend parallels that determined for the CX_3^+ (X = F, Cl, Br, I) series.

2.5. Topological analysis of the electron localization function

The topological analysis of the Becke and Edgecombe [67] electron localization function as formulated by Silvi and co-workers [68,69] leads to a robust description of chemical bonding based on the topological analyses of HF or DFT total electron density related to the Pauli exclusion principle. The ELF is a dimensionless function in three-space giving large values (0.5–1.0) for regions (basins) where electron density is localized. From the ELF function, the volume and electron population (N_i) values are calculated for each basin, i.e., one-center core C(A), two-center bonding V(A,B) or one-center non-bonding (''lone pair'') V(A) or V(B) basins. Basin lobes can be graphically presented as isosurfaces at a particular ELF value, thus showing where the bonding and non-bonding electrons are most likely located in a molecule. A lobe basin separation value (f_{sep}) can be assigned to each basin when the basin lobe clearly begins to separate from the remaining overlapping basins while systematically increasing the ELF value (f) of the graphical presentation. A basin having a low population contribution from other basins has a λ value of 0.01–0.45 and is considered to have its electrons localized, while $\lambda > 0.45$ indicates that the basin population has a large

[1] The experimental geometric parameters for $(CH_3)_2CF^+$ are taken from [21] and the values calculated in this work are given in square brackets: C–C, 1.413(13), 1.450(13) Å [1.431 Å]; C–F, 1.285(11) Å [1.319 Å]; ∠C–C–C, 126.1(8)°; [130.3°]; ∠F–C–C, 116.5(8)°, 117.3(8)°; [114.8°]. NBO natural charges: methyl C (−0.740), central C (0.922), F (−0.192). Valencies: methyl C (3.956), central C (4.000), F (1.836). Ionic bond orders: C–C (0.127), C–F (1.131).

contribution from other basins and thus its electrons are delocalized. The following chemical interpretations of the ELF results are only done in a semi-quantitave fashion because of the limited numerical accuracy of integration grids and the statistical nature of the ELF analyses (see Section 4).

ELF analyses do not lead to bond orders or basin populations that are comparable with NBO properties, nor can the values of basin populations from the ELF analyses of different systems be directly compared [70]. However, such analyses complement bonding descriptions by visualizing the statistical electron distribution resulting from a simple numerical integration of the total electron density. Fig. 2 depicts the lobes of ELF basins as isosurface plots at the ELF value of 0.70 along with their integrated basin volumes for the species considered in the present work. The ELF descriptions of the BX_3 and CX_3^+ series are considered in detail in the ensuing discussions whereas those of AlX_3 and SiX_3^+, $EX_3^{2-/-}$, $EX_3^{0/+}$ and $EX_3H^{-/0}$ (E = B, C, Al, Si and X = F, Cl, Br, I) are treated in a summary fashion. A more detailed listing of symmetry-averaged ELF parameters is provided in the Supporting information.

2.5.1. Planar $EX_3^{0/+}$ (D_{3h})

A summary of basin separation values, basin volumes (V), basin populations (N_i), relative fluctuations ($\lambda = \sigma^2/N_i$, where σ^2 is the variance of the basin population arising from contributions of other basins), and the contribution analyses (%) for the planar EX_3^+ and EX_3 series is provided in Table 3.

An overview of the ELF isosurfaces for the isovalent EX_3 and EX_3^+ (D_{3h}) species (Fig. 2) reveals several general trends. The B–X and C–X bond basin volumes, $V(B/C,X_i)$, increase almost linearly with decreasing Allred–Rochow electronegativity [71] of X (R^2: B, 0.968; Al, 0.954; C, 0.954; Si, 0.962). As well, the bond basin lobes contract towards the E atom as the electronegativity difference decreases. The E–X ionic bond orders (Table 1) also decrease in the same order indicating, that the bonding becomes more covalent over the series F < Cl < Br < I. The bond basin is completely absent for AlF_3 and small for SiF_3^+ (7.38), which is consistent with ionic bond orders (AlF_3, 1.151; SiF_3^+, 1.031) that are the highest among the EX_3 and EX_3^+ series. The non-bonding X basin volumes also increase along the same series, because the core electrons of the heavier halogen atoms more effectively shield the nuclear charge. The X basins, $V(X_i)$, are divided into two discreet basins that, however, join to form a common symmetric pear-shaped lobe when X = F. This lobe incrementally flattens, taking on a toroidal shape upon descending group 17.

A more detailed analysis of the ELF isosurfaces for the CX_3^+ and BX_3 series (Table 3) reveals that the central atom core basin lobes, $C(C)$ and $C(B)$, separate at very low ELF values (0.02–0.09) having low and almost constant λ values (B: 0.09, C: 0.11) arising from interactions with the bonding basins $V(E, X_i)$ (E = B,C). The halogen core basins $C(X)$ have low f_{sep} values (0.09–0.25) and basin volumes that increase with increasing numbers of core electrons. The core electrons are localized, having low λ values

Table 3
Symmetry-averaged ELF basin separation values (f_{sep}), basin volumes (V), basin populations (N_i), relative fluctuations (λ) and contributions (%) of other basins to the variances ($\sigma^2(N_i)$) for CX_3^+, BX_3, SiX_3^+, and ALX_3 (X = F, Cl, Br, I)[a]

Basin[b]	f_{sep}	V	N_i (e)	λ	Contribution analysis (%)[c]
CF_3^+ (D_{3h})					
$C(C)$	0.06	0.92	2.07	0.12	23% $V(C,F_i)$; 23% $V(C,F_j)$; 23% $V(C,F_k)$
$C(F_i)$	0.14	0.16	2.03	0.22	41% $V_1(F_i)$; 46% $V_2(F_i)$; 10% $V(C,F_i)$
$V(C,F_i)$	0.79	10.9	1.56	0.63	34% $V_1(F_i)$; 36% $V_2(F_i)$
$V_1(F_i)$	0.88	47.3	3.13	0.43	14% $C(F_i)$; 54% $V_2(F_i)$; 25% $V(C,F_i)$
$V_2(F_i)$	0.88	47.1	3.25	0.43	15% $C(F_i)$; 52% $V_1(F_i)$; 25% $V(C,F_i)$
CCl_3^+ (D_{3h})					
$C(C)$	0.05	0.86	2.08	0.11	25% $V(C,Cl_i)$; 25% $V(C,Cl_j)$; 25% $V(C,Cl_k)$
$C(Cl_i)$	0.09	2.27	10.06	0.05	41% $V_1(Cl_i)$; 42% $V_2(Cl_i)$; 15% $V(C,Cl_i)$
$V(C,Cl_i)$	0.76	20.9	1.97	0.55	28% $V_1(Cl_i)$; 28% $V_2(Cl_i)$; 10% $V(C,Cl_j)$; 10% $V(C,Cl_k)$
$V_1(Cl_i)$	0.91	105.3	2.95	0.43	17% $C(Cl_i)$; 48% $V_2(Cl_i)$; 24% $V(C,Cl_i)$
$V_2(Cl_i)$	0.91	105.9	2.99	0.43	17% $C(Cl_i)$; 48% $V_1(Cl_i)$; 24% $V(C,Cl_i)$
CBr_3^+ (D_{3h})					
$C(C)$	0.05	0.85	2.08	0.11	27% $V(C,Br_i)$; 27% $V(C,Br_j)$; 27% $V(C,Br_k)$
$C(Br_i)$	0.15	5.23	27.74	0.04	43% $V_1(Br_i)$; 44% $V_2(Br_i)$; 12% $V(C,Br_i)$
$V(C,Br_i)$	0.70	25.8	2.05	0.55	12% $C(Br_i)$; 24% $V_1(Br_i)$; 24% $V_2(Br_i)$; 12% $V(C,Br_j)$; 12% $V(C,Br_k)$
$V_1(Br_i)$	0.89	130.4	3.07	0.47	34% $C(Br_i)$; 38% $V_2(Br_i)$; 18% $V(C,Br_i)$
$V_2(Br_i)$	0.89	130.9	3.11	0.47	35% $C(Br_i)$; 38% $V_1(Br_i)$; 18% $V(C,Br_i)$
CI_3^+ (D_{3h})[d]					
$C(C)$	0.05	0.85	2.08	0.11	27% $V(C,I_i)$; 27% $V(C,I_j)$; 27% $V(C,I_k)$
$V(C,I_i)$	0.70	31.0	1.96	0.53	26% $V_1(I_i)$; 26% $V_2(I_i)$; 14% $V(C,I_j)$; 14% $V(C,I_k)$
$V_1(I_i)$	0.93	181.4	2.99	0.37	60% $V_2(I_i)$; 24% $V(C,I_i)$
$V_2(I_i)$	0.93	181.8	3.00	0.37	60% $V_1(I_i)$; 24% $V(C,I_i)$

Table 3 (*Continued*)

Basin[b]	f_{sep}	V	N_i (e)	λ	Contribution analysis (%)[c]
BF_3 (D_{3h})					
C(B)	0.07	1.74	2.07	0.09	21% V(B,F$_i$); 21% V(B,F$_j$); 21% V(B,F$_k$)
C(F$_i$)	0.25	0.17	2.14	0.17	43% V_1(F$_i$); 44% V_2(F$_i$); 14% V(B,F$_i$)
V(B,F$_i$)	0.82	12.0	1.47	0.62	39% V_1(F$_i$); 39% V_2(F$_i$)
V_1(F$_i$)	0.87	55.7	3.16	0.42	12% C(F$_i$); 56% V_2(F$_i$); 26% V(B,F$_i$)
V_2(F$_i$)	0.87	56.3	3.22	0.42	12% C(F$_i$); 56% V_1(F$_i$); 27% V(B,F$_i$)
BCl_3 (D_{3h})					
C(B)	0.09	1.76	2.06	0.09	22% V(B,Cl$_i$); 22% V(B,Cl$_j$); 22% V(B,Cl$_k$)
C(Cl$_i$)	0.09	2.26	10.06	0.05	40% V_1(Cl$_i$); 41% V_2(Cl$_i$); 17% V(B,Cl$_i$)
V(B,Cl$_i$)	0.81	26.1	1.84	0.56	33% V_1(Cl$_i$); 34% V_2(Cl$_i$)
V_1(Cl$_i$)	0.90	121.1	3.01	0.44	17% C(Cl$_i$); 50% V_2(Cl$_i$); 26% V(B,Cl$_i$)
V_2(Cl$_i$)	0.90	121.7	3.05	0.44	17% C(Cl$_i$); 50% V_1(Cl$_i$); 26% V(B,Cl$_i$)
BBr_3 (D_{3h})					
C(B)	0.02	1.76	2.06	0.09	22% V(B,Br$_i$); 22% V(B,Br$_j$); 22% V(B,Br$_k$)
C(Br$_i$)	0.17	5.23	27.75	0.04	42% V_1(Br$_i$); 42% V_2(Br$_i$); 15% V(B,Br$_i$)
V(B,Br$_i$)	0.77	32.0	1.93	0.57	16% C(Br$_i$); 29% V_1(Br$_i$); 29% V_2(Br$_i$)
V_1(Br$_i$)	0.86	146.8	3.13	0.48	32% C(Br$_i$); 41% V_2(Br$_i$); 21% V(B,Br$_i$)
V_2(Br$_i$)	0.86	147.3	3.15	0.48	32% C(Br$_i$); 41% V_1(Br$_i$); 21% V(B,Br$_i$)
BI_3 (D_{3h})[d]					
C(B)	0.02	1.77	2.06	0.09	22% V(B,I$_i$); 22% V(B,I$_j$); 22% V(B,I$_k$)
V(B,I$_i$)	0.79	38.12	1.79	0.54	33% V_1(I$_i$); 33% V_2(I$_i$)
V_1(I$_i$)	0.92	195.1	3.06	0.38	63% V_2(I$_i$); 27% V(B,I$_i$)
V_2(I$_i$)	0.92	195.5	3.09	0.38	62% V_1(I$_i$); 27% V(B,I$_i$)
SiF_3^+ (D_{3h})					
C(Si)	0.02	7.44	10.0	0.03	12% V_1(F$_{i,j,k}$); 12% V_1(F$_{i,j,k}$)
C(F$_i$)	0.13	0.18	2.14	0.18	44% V_1(F$_i$); 44% V_2(F$_i$)
V_1(Si,F$_i$)	0.83	0.55	0.21	0.92	38% V_1(F$_i$); 20% V_2(F$_i$); 12% V_2(Si,F$_i$)
V_2(Si,F$_i$)	0.83	6.38	0.41	0.86	39% V_1(F$_i$); 40% V_2(F$_i$)
V_1(F$_i$)	0.88	60.9	3.58	0.40	12% C(F$_i$); 66% V_2(F$_i$); 10% V_2(Si,F$_i$)
V_2(F$_i$)	0.88	62.0	3.65	0.40	12% C(F$_i$); 66% V_1(F$_i$); 10% V_2(Si,F$_i$)
$SiCl_3^+$ (D_{3h})					
C(Si)	0.03	7.03	10.01	0.04	26% V(Si,Cl$_i$); 26% V(Si,Cl$_j$); 26% V(Si,Cl$_k$)
C(Cl$_i$)	0.08	2.27	10.06	0.05	40% V_1(Cl$_i$); 41% V_2(Cl$_i$); 17% V(Si,Cl$_i$)
V(Si,Cl$_i$)	0.82	40.6	1.97	0.57	35% V_1(Cl$_i$); 35% V_2(Cl$_i$)
V_1(Cl$_i$)	0.90	116.1	2.96	0.45	16% C(Cl$_i$); 49% V_2(Cl$_i$); 29% V(Si,Cl$_i$)
V_2(Cl$_i$)	0.90	116.8	3.00	0.45	16% C(Cl$_i$); 49% V_1(Cl$_i$); 29% V(Si,Cl$_i$)
$SiBr_3^+$ (D_{3h})					
C(Si)	0.04	6.94	10.01	0.04	14% V_1(Si,Br$_{i,j,k}$); 14% V_2(Si,Br$_{i,j,k}$)
C(Br$_i$)	0.14	5.42	27.83	0.04	41% V_1(Br$_i$); 41% V_2(Br$_i$)
V_1(Si,Br$_i$)	0.78	23.9	1.02	0.73	12% C(Br$_i$); 24% V_1(Br$_i$); 24% V_2(Br$_i$); 22% V_2(Si,Br$_i$)
V_2(Si,Br$_i$)	0.78	24.5	1.07	0.72	12% C(Br$_i$); 24% V_1(Br$_i$); 24% V_2(Br$_i$); 21% V_1(Si,Br$_i$)
V_1(Br$_i$)	0.87	141.1	3.01	0.50	32% C(Br$_i$); 39% V_2(Br$_i$); 12% V_1(Si,Br$_i$); 12% V_2(Si,Br$_i$)
V_2(Br$_i$)	0.87	141.7	3.05	0.50	32% C(Br$_i$); 39% V_1(Br$_i$); 12% V_1(Si,Br$_i$); 12% V_2(Si,Br$_i$)
SiI_3^+ (D_{3h})[d]					
C(Si)	0.04	6.86	10.01	0.04	25% V(Si,I$_i$); 25% V(Si,I$_j$); 25% V(Si,I$_k$)
V(Si,I$_i$)	0.79	52.7	1.84	0.57	35% V_1(I$_i$); 35% V_2(I$_i$)
V_1(I$_i$)	0.92	199.2	3.05	0.39	61% V_2(I$_i$); 30% V(Si,I$_i$)
V_2(I$_i$)	0.92	199.9	3.08	0.39	61% V_1(I$_i$); 30% V(Si,I$_i$)
AlF_3 (D_{3h})					
C(Al)	0.01	12.1	10.04	0.03	13% V_1(F$_{i,j,k}$); 17% V_2(F$_{i,j,k}$)
C(F$_i$)	0.13	0.18	2.15	0.18	48% V_1(F$_i$); 50% V_2(F$_i$)
V_1(F$_i$)	0.87	74.8	3.87	0.38	13% C(F$_i$); 83% V_2(F$_i$)
V_2(F$_i$)	0.87	70.5	3.96	0.38	13% C(F$_i$); 81% V_1(F$_i$)
$AlCl_3$ (D_{3h})					
C(Al)	0.02	12.2	10.04	0.03	23% V(Al,Cl$_i$); 23% V(Al,Cl$_j$); 23% V(Al,Cl$_k$)
C(Cl$_i$)	0.08	2.27	10.06	0.05	43% V_1(Cl$_i$); 44% V_2(Cl$_i$); 20% V(Al,Cl$_i$)
V(Al,Cl$_i$)	0.84	49.5	1.89	0.57	37% V_1(Cl$_i$); 37% V_2(Cl$_i$)
V_1(Cl$_i$)	0.90	128.2	3.00	0.45	16% C(Cl$_i$); 51% V_2(Cl$_i$); 20% V(Al,Cl$_i$)
V_2(Cl$_i$)	0.90	128.0	3.02	0.45	16% C(Cl$_i$); 51% V_1(Cl$_i$); 29% V(Al,Cl$_i$)

Table 3 (*Continued*)

Basin[b]	f_{sep}	V	N_i (e)	λ	Contribution analysis (%)[c]
$AlBr_3$ (D_{3h})					
C(Al)	0.02	12.3	10.05	0.03	10% V_1(Al,Br$_{i,j,k}$); 14% V_2(Al,Br$_{i,j,k}$)
C(Br$_i$)	0.15	5.46	27.84	0.04	40% V_1(Br$_i$); 41% V_2(Br$_i$); 10% V_2(Al,Br$_i$)
V_1(Al,Br$_i$)	0.81	29.7	0.99	0.73	14% C(Br$_i$); 26% V_1(Br$_i$); 26% V_2(Br$_i$); 21% V_2(Al,Br$_i$)
V_2(Al,Br$_i$)	0.81	30.2	1.04	0.74	15% C(Br$_i$); 26% V_1(Br$_i$); 26% V_2(Br$_i$); 20% V_1(Al,Br$_i$)
V_1(Br$_i$)	0.87	157.6	3.04	0.50	31% C(Br$_i$); 41% V_2(Br$_i$); 12% V_1(Al,Br$_i$); 13% V_2(Al,Br$_i$)
V_2(Br$_i$)	0.87	157.9	3.07	0.50	31% C(Br$_i$); 41% V_1(Br$_i$); 12% V_1(Al,Br$_i$); 13% V_2(Al,Br$_i$)
AlI_3 (D_{3h})[d]					
C(Al)	0.02	12.2	10.06	0.03	24% V(Al,I$_i$); 24% V(Al,I$_j$); 24% V(Al,I$_k$)
V(Al,I$_i$)	0.83	64.1	1.70	0.57	39% V_1(I$_i$); 39% V_2(I$_i$)
V_1(I$_i$)	0.91	213.4	3.13	0.40	64% V_2(I$_i$); 31% V(Al,I$_i$)
V_2(I$_i$)	0.91	213.9	3.13	0.40	63% V_1(I$_i$); 30% V(Al,I$_i$)

[a] HF/(SDB-)cc-pVTZ//MP2/(SDB-)cc-pVTZ. The electron contribution coming from a specific basin can be estimated by solving the variance σ^2 (=λN_i) and then calculating the percentage of the variance coming from the contributing basin.

[b] Index: i = 1–3; for i = 1: j = 2, k = 3; for i = 2: j = 1, k = 3; for i = 3: j = 1, k = 2; l = 4–15. F$_{i,A}$ (i = 1–3) denote axial fluorines while F$_{l,B}$ (l = 4–15) denote equatorial fluorines.

[c] Contributions lower than 10% have been omitted from this table because of the low accuracies of the population analyses.

[d] There are no core basins given for iodine or tellurium because pseudo-potential basis sets were used.

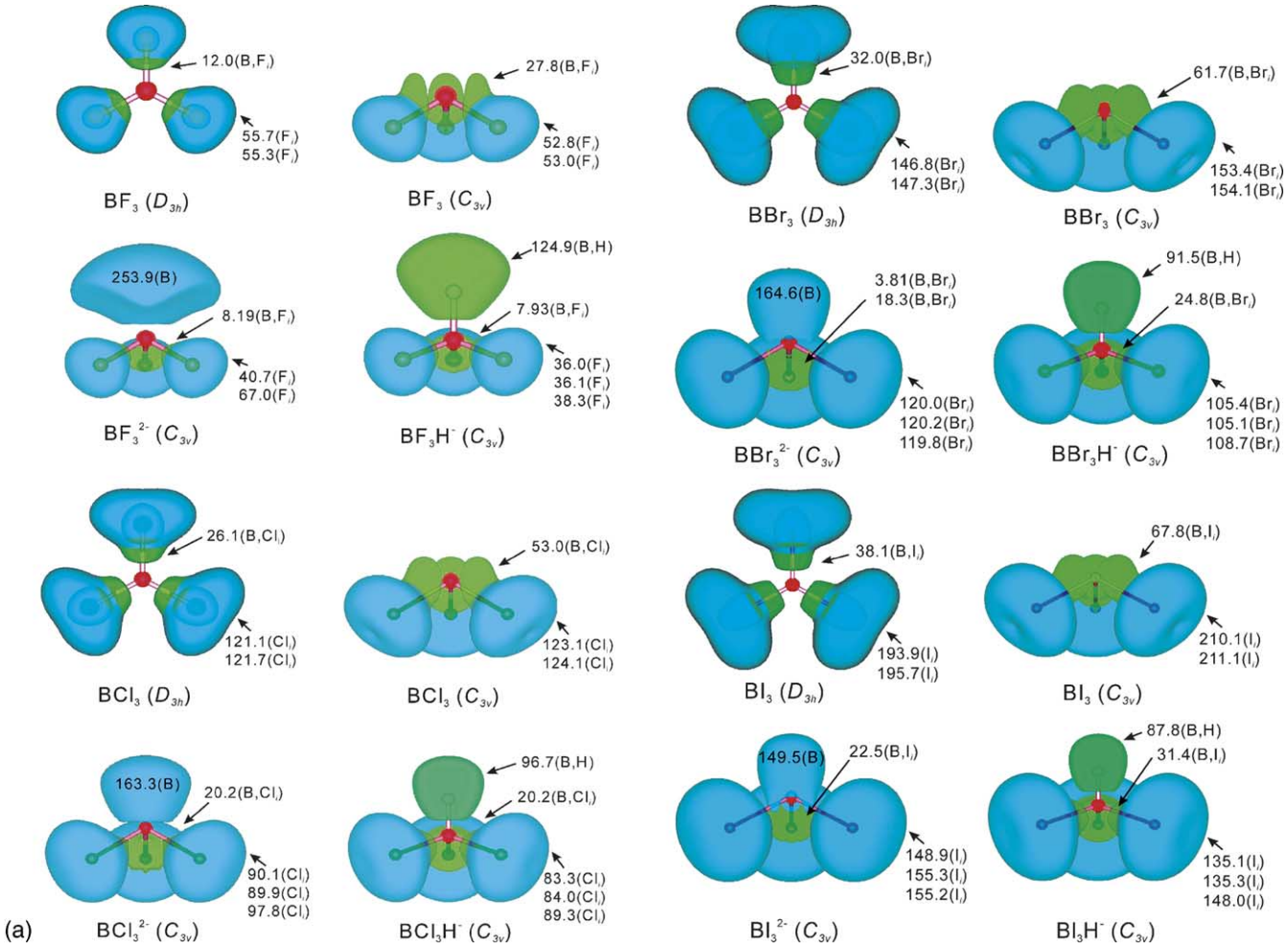

Fig. 2. ELF isosurface plots at the 0.70 contour level for $EX_3^{0/+}$ (D_{3h}), $EX_3^{2-/-}$, $EX_3^{0/+}$ (C_{3v}) and $EX_3H^{-/0}$ (E = B, C, Al, Si and X = F, Cl, Br, I) at the HF/(SDB-)cc-pVTZ//MP2/(SDB-)cc-pVTZ level. Color scheme: blue, monosynaptic (non-bonding "lone pair") basin, V(X$_i$) and V(E); green, bisynaptic (bonding) basin, V(E,X$_i$); red, core basin, C(E). Values shown are for the basin volumes (arbitrary units) of V(X$_i$) and V(E,X$_i$).

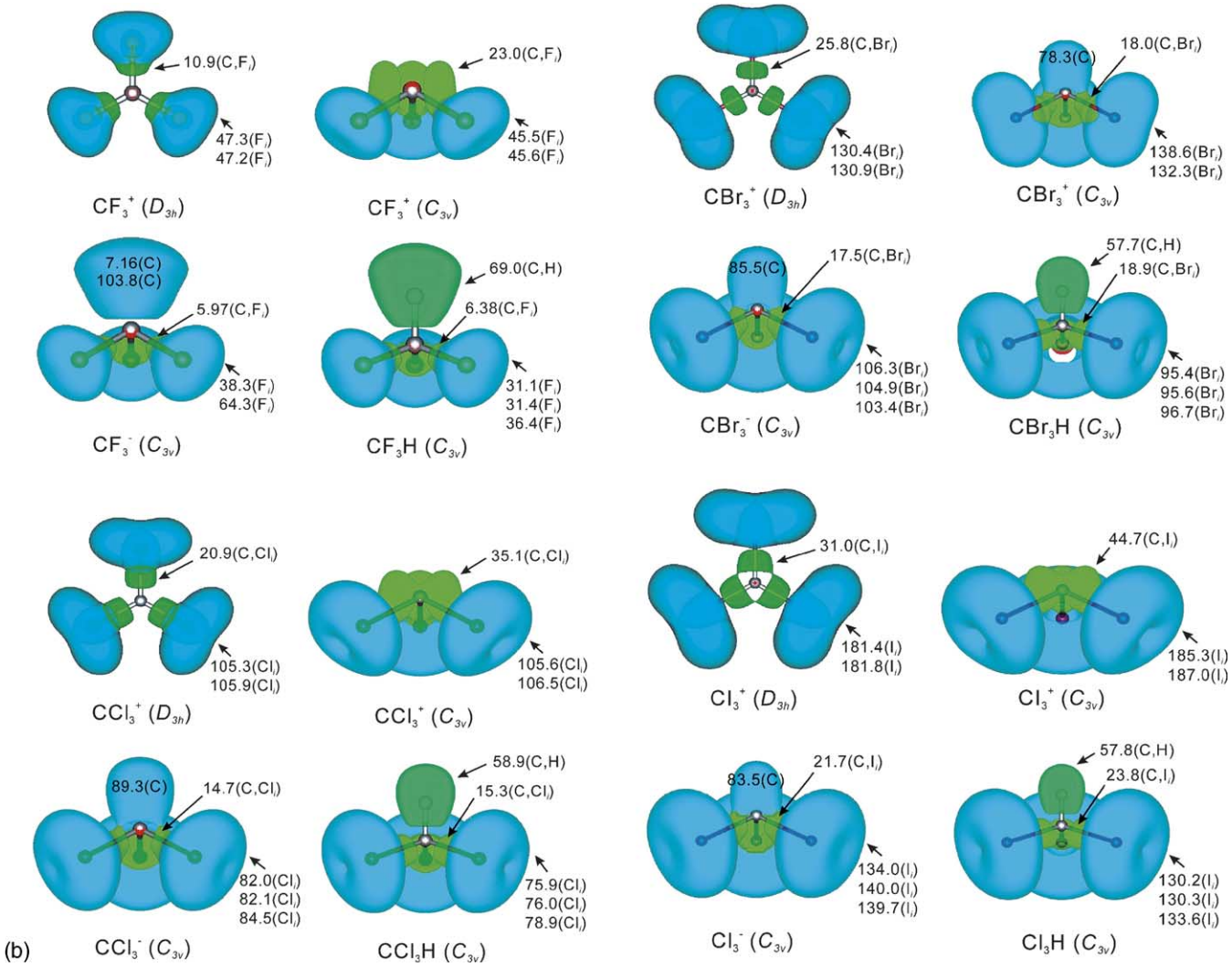

Fig. 2. (*Continued*).

(<0.17), with the fluorine atom having the highest value (0.17), which mainly arises from interactions with the non-bonding basins of the fluorine atom, $V(F_i)$. For the remaining halogens with a higher core electron count, the relative fluctuations drop to a low value (Cl: 0.05; Br: 0.04).

The basins that are mainly occupied by the valence electrons are the bond basins $V(E,X_i)$ and the non-bonding electron lone pair basins $V(X_i)$. The CF_3^+/BF_3 bond basins $V(E,F_i)$ separate out of the lone pair basins at higher f_{sep} values (0.79/0.82) than those of the remaining CX_3^+/BX_3 species (Cl: 0.76/0.81, Br: 0.70/0.77, I: 0.70/0.79). The $V(E,F_i)$ basins interact strongly with the fluorine lone pair basins $V(F_i)$ so that more than half ($\lambda = 0.63/0.62$) of the bond basin population (1.54/1.42 e) comes from the lone pairs (0.68/0.71 e), which is indicative of the ionic characters of the E–F bonds. The bond basin populations of CCl_3^+, CBr_3^+ and CI_3^+ are higher than the populations of $V(C,F_i)$ and have lower λ values, so there is less interaction with their lone pair basins, $V(X_i)$. In the case of CCl_3^+, the C–Cl bonds provide small contributions (10%, 0.20 e). The interactions between bond basins are 12% (0.24 e) and 14% (0.29 e) in CBr_3^+ and CI_3^+, respectively. Again, the bond basin populations of BCl_3, BBr_3 and BI_3 are higher than that of BF_3 with somewhat lower λ values, but in this case the interactions with other bond basins are even smaller (less than 10% for each species; see footnote c in Table 3). The $V(E,X_i)$ bonding basins have λ values of 0.53–0.63 (Table 3) and a substantial fraction of their electron populations comes from non-bonding basins located on the halogens as shown in Fig. 2. In the case of fluorine, the bonding lobes are close to the non-bonding lobes, corresponding to bonds that are highly polar. As the electronegativity of X decreases, the average $V(E,X_i)$ bond basin population increases and the corresponding lobes move towards the central atom, in accord with increasing $X \rightarrow E$ back-donation and increasing positive natural charge on the halogen [1,2,5,21,25–27,59]. The bond basins increase their populations by removing electron density from halogen lone-pair basins, thereby increasing the covalent component and decreasing the ionic component,

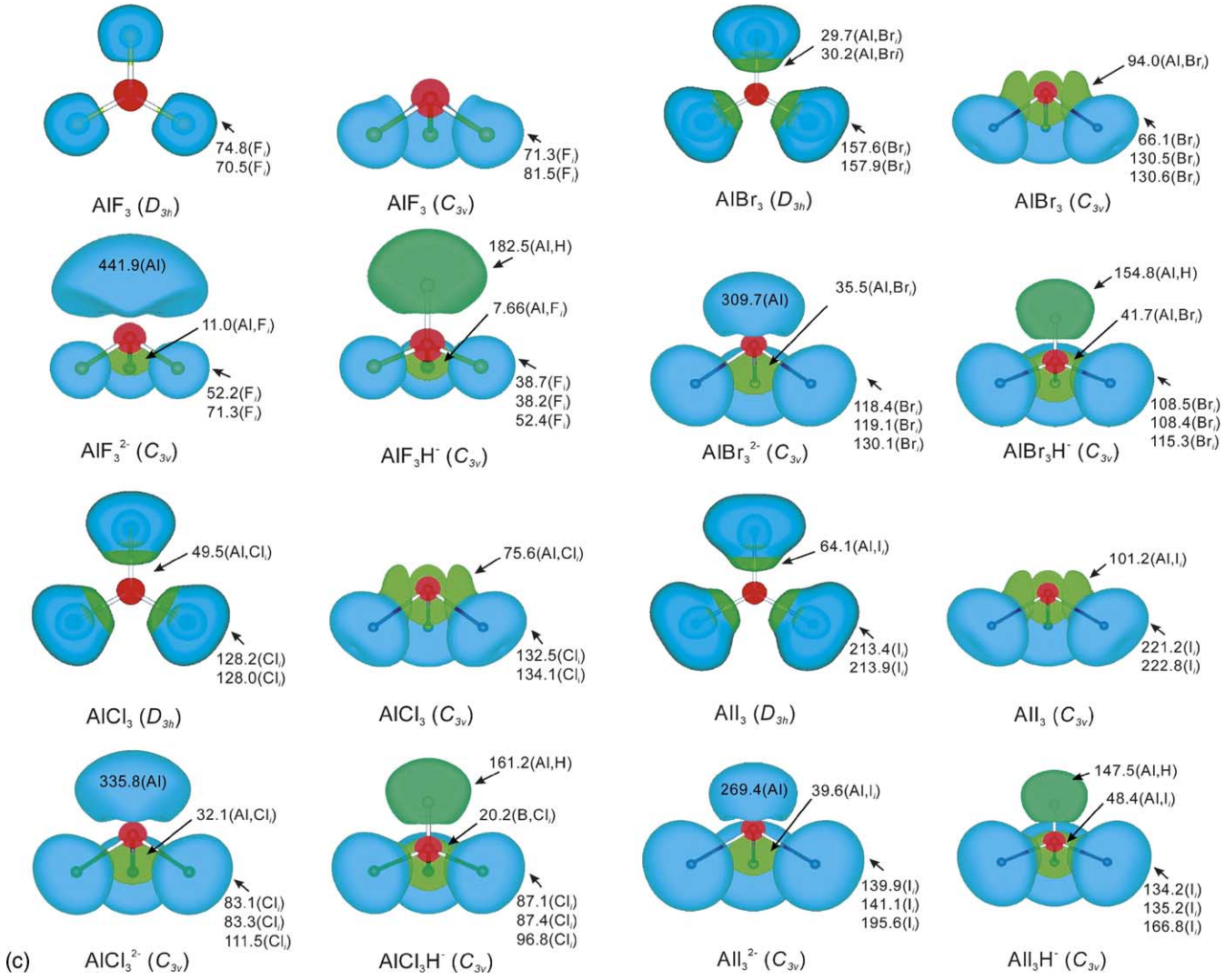

Fig. 2. (*Continued*).

so that the E–X bond strengths decrease in the order F > Cl > Br > I over both series.

2.5.2. $EX_3^{0/+}$ (C_{3v})

Geometric changes from planar to pyramidal (Scheme 1, step (a)) nearly double the bond basin volumes for E = B and C, while non-bonding basin volumes increase only slightly for X = Cl (2%), Br (5%), I (8%), but decrease by 5% for X = F. The bond basin lobes distort towards E atom towards the peak of the pyramid to compensate for the electron deficit created above the E atom by the geometry change. This is most evident in BF_3 where the volumes of the bonding lobes, $V(B,X_i)$, are more sharply defined than in the other BX_3 molecules and project well above the boron atom. The electron densities of these lobes make the addition of an electron pair to the trigonal pyramidal conformation more difficult, resulting in lower EPA and Lewis acidity values for BF_3. These volumes become more diffuse upon descending group 17, in agreement with the Lewis acidity trend for BX_3 (F < Cl < Br < I).

In contrast, the C–F bond lobes, $V(C,X_i)$, in CF_3^+ are more diffuse than in BF_3, which accounts for, in part, why CF_3^+ is a stronger Lewis acid than BF_3. As well, the bonding basins become more concentrated above the carbon atom, which is most evident for CBr_3^+, where the C–Br bond basins approach each other so closely during pyramidalization that a ''pre-lone pair'' basin lobe is formed on the carbon atom that is directed away from the tripodal plane. This behavior is in agreement with the EPA trend calculated for CX_3^+ (F > Cl > Br > I). It is interesting to note that the charges on carbon in pyramidal CBr_3^+ (−0.552) and CBr_3^- (−0.514) and their respective lone pair volumes (78.3 and 85.5) are very similar.

For $EX_3^{0/+}$ (E = Al,Si), the ELF diagrams show features that are similar to those of their row 2 analogues. The lack of bonding basins, $V(Al/Si,F_i)$, where X = F, may account for

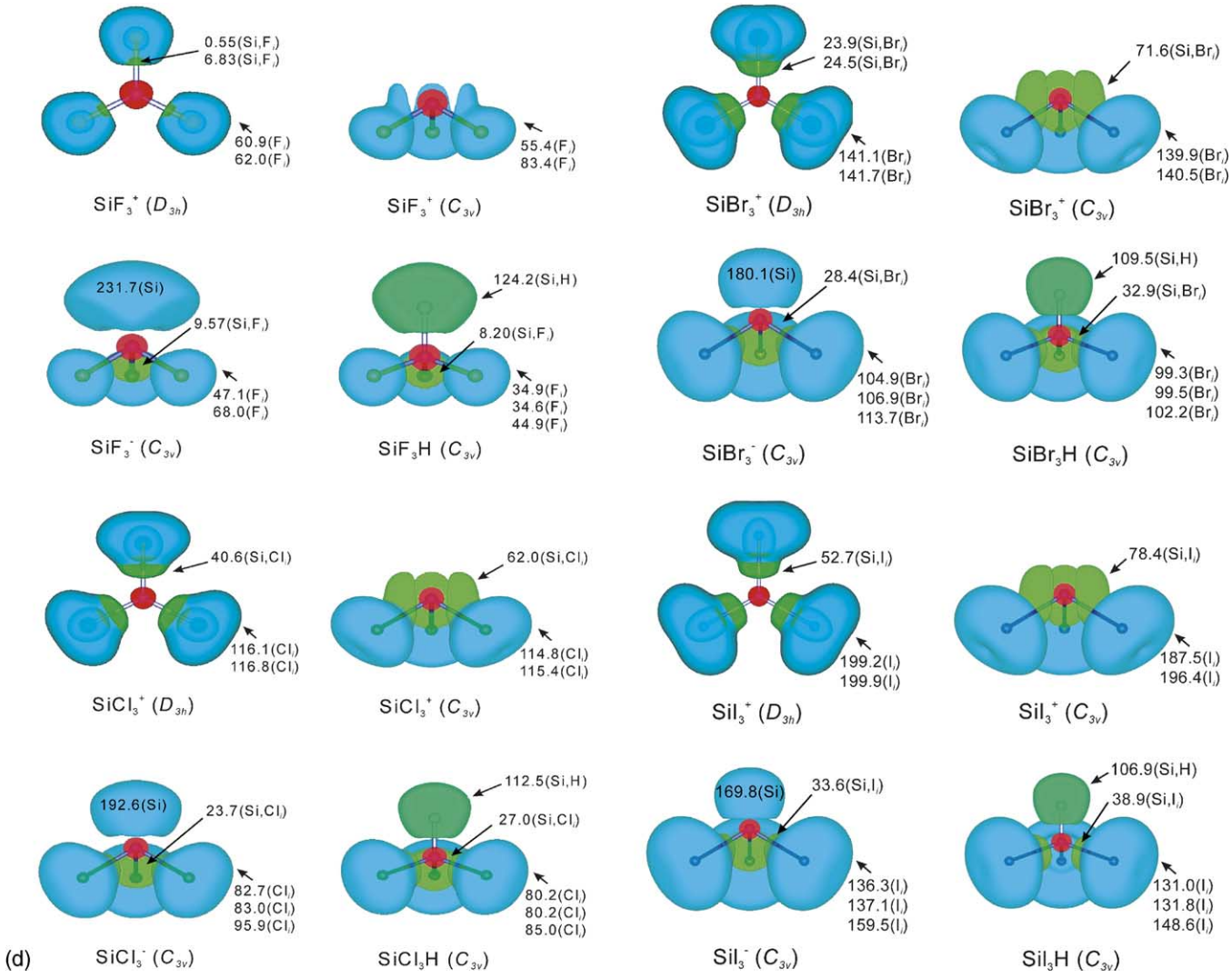

Fig. 2 (*Continued*).

why these species are stronger Lewis acids on the EPA scale than the corresponding BF_3 and CF_3^+ species.

2.5.3. $EX_3^{2-/-}$ (C_{3v})

Within the BX_3^{2-} series, the volume of the relatively large lone pair basin, V(B), is clearly larger than its halogen counterparts, $V(X_i)$. The basin lobe is located well above the apical boron atom and is considerably more diffuse than those of its higher halogen congeners, which is consistent with the low EPA of planar BF_3. The basin volumes, when plotted against the electronegativity of X, linearly decrease ($R^2 = 0.956$) upon descending group 17, with the corresponding lobes becoming progressively less diffuse and further displaced toward the boron atom. The net effect is that the lone pair is progressively integrated into the electronic structure of the anion, making it less accessible and thus lowering the Lewis basicity of the anion.

The CX_3^- series follow the same trend as the BX_3^{2-} series. As in the BX_3^{2-} series, the volume of the lone pair basin on the carbon atom of CF_3^- is the largest within the CX_3^- series and also displays a near-linear relationship between the lone pair basin volume and the electronegativity of X ($R^2 = 0.956$). The AlX_3^{2-} and SiX_3^- isosurface plots show topological trends that are similar to those of their boron and carbon analogues, with plots of the lone pair volume on the E atom versus the electronegativity of X showing excellent linear correlations (Al, $R^2 = 0.990$; Si, $R^2 = 0.977$).

2.5.4. $EX_3H^{-/0}$ (C_{3v})

The E–H bond basin is topologically treated as a special case [69] because hydrogen does not possess core electrons, accounting for why the E–H bond lobes appear to be closer to their respective hydrogen atoms and have shapes similar to the non-bonding lobes on the E atom. The ELF diagrams of $EX_3H^{-/0}$ and $EX_3^{2-/-}$ are very similar in appearance, with the hydrogen atom appearing to have been squeezed into the lone pair of the corresponding trigonal pyramidal

anion. Comparisons of $EX_3H^{-/0}$ and $EX_3^{2-/-}$ demonstrate that as the E–X bonds lengthen upon descending group 17, more space is provided for the E–H bond pair and the lone pair on E to move closer to the E atom in the same order. Thus, lone pair availability on $EX_3^{2-/-}$ correspondingly reduced and is consistent with the proton affinity order calculated above (see Section 2.3). The opposite trends in EPA and proton affinity values for the carbon and silicon series indicate that CF_3^+ and SiF_3^+ are the strongest acids in their respective series and that their two-electron reduction products, CF_3^- and SiF_3^-, are the strongest bases.

3. Conclusions

Electron pair affinities introduced in this work have been shown to provide near-linear correlations with previously calculated fluoride ion affinities and hydride ion affinities for $EX_3^{0/+}$ (E = B, C, Al, Si; X = F, Cl, Br, I) as well as being in good agreement with experimental Lewis acidity trends. Lewis acidity trends derived from the calculated electron pair affinities of EX_3 and EX_3^+ indicate that the Lewis acidities are dominated by the pyramidalization energies for the BX_3 and AlX_3 series, and by the electron attachment energies for the CX_3^+ and SiX_3^+ cation series. This suggests that a ''Lewis base-free'' approach to a relative Lewis acidity scale may be derived that is widely applicable.

Natural valencies, natural bond orders and natural charges have been useful in assessing the bonding in these species in combination with the visual representations of electron localization function isosurface lobes and the lobe volumes. The calculated NBO charges on carbon and the ligand atoms of the CX_3^+ cations (X = Cl, Br, I, $OTeF_5$) can be correlated with the secondary contacts in their crystal structures. The trigonal planar carbon centers are, in the majority of cases (X = Cl, Br, and I), well isolated from the fluorine ligand atoms of their respective weakly coordinating anions and/or SO_2ClF present in the crystal lattice when the calculated charge on carbon is negative. The positively charged halogen ligands of these cations display correspondingly short X···F and X···O contacts with their anions and SO_2ClF. In the cases of $C(OTeF_5)_3^+$, $(CH_3)_2CF^+$ and related fluoro-cations, the central carbon atoms have calculated charges that are positive, resulting in carbon centers that have trigonal bipyramidal coordination as a result of short C···O and C···F contacts to SO_2ClF or to fluorine atoms of their AsF_6^- and $As_2F_{11}^-$ anions.

Electron localization function treatments provide good descriptions of the total electron density, and demonstrate that the E–F bonds of EF_3 and EF_3^+ are the most ionic. The ELF isosurfaces of the pyramidalized series of Lewis acids, $EX_3^{0/+}$ (C_{3v}), show that the electron density of the bonding lobes that project above the apical central atom, $V(E, X_i)$, correlates with the ability of $EX_3^{0/+}$ (C_{3v}) to accept an electron pair, and is consistent with the EPA order calculated for each series.

4. Experimental

All electron structure calculations were carried out using the Gaussian 98 set of programs [72]. Geometries were fully optimized using D_{3h} and C_{3v} symmetries at the MP2 level of theory. Dunning's correlation consistent basis sets of triple-zeta quality, cc-pVTZ, were used for all atoms except iodine, for which a quasi-relativistic large core effective core potential was used with a corresponding triple-zeta valence basis set, SDB-cc-pVTZ. All basis sets were used as they are referenced in the EMSL basis set library [73]. The combined use of basis sets is indicated as (SDB-)cc-pVTZ, meaning that cc-pVTZ was used for all atoms other than iodine for which SDB-cc-pVTZ was used. Single point coupled cluster calculations using both single and double substitutions including non-iterative triple excitations, CCSD(T), were used for all optimized geometries. All methods were used as they are implemented in Gaussian 98 [72]. Natural bond orbital (NBO) [61] and natural resonance theory (NRT) [63] analyses were carried out at the MP2/(SDB-)cc-pVTZ//MP2/(SDB-)cc-pVTZ level using the program NBO, version 5.0 [61]. Topological electron localization function analyses [68,69] were carried out using the TopMod set of programs [74]. Visualization of the ELF isosurface lobes was accomplished by use of GopenMol [75].

Acknowledgements

We thank the donors of the Petroleum Research Fund, administered by the American Chemical Society, for support of this work under ACS-PRF No. 40959-AC3 (G.J.S.) as well as the Natural Sciences and Engineering Research Council of Canada for the award of a graduate scholarship (M.D.M.) and for support in the form of a research grant (G.J.S.). We also thank the Finnish IT Center for Science for the use of their computing resources (R.J.S.).

Supplementary information available

Supplementary information associated with this article consisting of Energies (Table S1) and NBO and ELF parameters (Table S2) can be found, in the online version, at doi:10.1016/j.jfluchem.2004.08.008.

References

[1] H.P.A. Mercier, M.D. Moran, G.J. Schrobilgen, C. Steinberg, R.J. Suontamo, J. Am. Chem. Soc. 126 (2004) 5533–5548.
[2] I. Krossing, A. Bihlmeier, I. Raabe, N. Trapp, Angew. Chem. Int. Ed. Engl. 42 (2003) 1531–1534.
[3] H. Vančik, K. Percač, D.E. Sunko, J. Am. Chem. Soc. 112 (1990) 7418–7419.
[4] G.A. Olah, L. Heiliger, G.K.S. Prakash, J. Am. Chem. Soc. 111 (1989) 8020–8021.

[5] G. Frenking, S. Fau, C.M. Marchand, H. Grützmacher, J. Am. Chem. Soc. 119 (1997) 6648–6655.
[6] M. Kaupp, O.L. Malkina, V.G. Malkin, Chem. Phys. Lett. 265 (1997) 55–59.
[7] C.H. Reynolds, J. Chem. Soc., Chem. Commun. (1991) 975–976.
[8] D.A. Dixon, D. Feller, G. Sandrone, J. Phys. Chem. A 103 (1999) 4744–4751.
[9] A. Ricca, J. Phys. Chem. A 103 (1999) 1876–1879.
[10] A. Hansel, Ch. Scheiring, M. Glantschnig, W. Lindinger, E.E. Ferguson, J. Chem. Phys. 109 (1998) 1748–1750.
[11] H. Basch, T. Hoz, S. Hoz, J. Phys. Chem. A 103 (1999) 6458–6467.
[12] C.F. Rodriquez, D.K. Bohme, A.C. Hopkinson, J. Phys. Chem. 100 (1996) 2942–2949.
[13] E.S.J. Robles, P. Chen, J. Phys. Chem. 98 (1994) 6919–6923.
[14] V. Jonas, G. Frenking, M.T. Reetz, J. Am. Chem. Soc. 116 (1994) 8741–8753.
[15] K.R.S. Chandrakumar, S. Pal, J. Phys. Chem. A 106 (2002) 11775–11781.
[16] B.D. Rowsell, R.J. Gillespie, G.L. Heard, Inorg. Chem. 38 (1999) 4659–4662.
[17] C.W. Bauschlicher Jr., A. Ricca, J. Phys. Chem. A 103 (1999) 4313–4318.
[18] S. Fau, G. Frenking, Mol. Phys. 96 (1999) 519–527.
[19] T. Brinck, J.S. Murray, P. Politzer, Inorg. Chem. 32 (1993) 2622–2625.
[20] K.K. Irikura, J. Am. Chem. Soc. 121 (1999) 7689–7695.
[21] K.O. Christe, X. Zhang, R. Bau, J. Hegge, G.A. Olah, G.K.S. Prakash, J.A. Sheehy, J. Am. Chem. Soc. 122 (2000) 481–487.
[22] J.W. Hudgens, R.D. Johnson III, B.P. Tsai, S.A. Kafafi, J. Am. Chem. Soc. 112 (1990) 5763–5772.
[23] H. Tachikawa, J. Phys. Chem. A 101 (1997) 7454–7459.
[24] M.E. Jacox, D.E. Milligan, J. Chem. Phys. 54 (1971) 3935–3950.
[25] K.O. Christe, B. Hoge, J.A. Boatz, G.K.S. Prakash, G.A. Olah, J.A. Sheehy, Inorg. Chem. 38 (1999) 3132–3142.
[26] E.A. Robinson, S.A. Johnson, T.-H. Tang, R.J. Gillespie, Inorg. Chem. 36 (1997) 3022–3030.
[27] E.A. Robinson, G.L. Heard, R.J. Gillespie, J. Mol. Struct. 485–486 (1999) 305–319.
[28] N.N. Greenwood, A. Earnshaw, Chemistry of the Elements, 2nd ed. Butterworth-Heinemann, Jordan Hill, Oxford, 1984, pp. 195–196.
[29] G.L. Miessler, D.A. Tarr, Inorganic Chemistry, 3rd ed. Pearson Prentice Hall, Upper Saddle River, NJ, 1991, pp. 154–157.
[30] G. Rayner-Canham, Descriptive Inorganic Chemistry, 2nd ed. W.H. Freeman and Company, New York, NY, 2000, pp. 230–231.
[31] C.E. Housecroft, A.G. Sharpe, Inorganic Chemistry, Pearson Education Ltd., Harlow, Essex, 2001, pp. 96–97, 25257–25558.
[32] F. Bessac, G. Frenking, Inorg. Chem. 42 (2003) 7990–7994.
[33] J.S. Hartman, J.M. Miller, Adv. Inorg. Chem. Radiochem. 21 (1978) 147–177.
[34] D.F. Shriver, B. Swanson, Inorg. Chem. 10 (1971) 1354–1365.
[35] H.C. Brown, R.R. Holmes, J. Am. Chem. Soc. 78 (1956) 2173–2176.
[36] C.S. Sreekanth, C.Y. Mok, H.H. Huang, K.L. Tan, J. Electron Spectrosc. Relat. Phenom. 58 (1992) 129–140.
[37] E.W. Rothe, B.P. Mathur, G.P. Reck, Inorg. Chem. 19 (1980) 829–831.
[38] A.Y. Timoshkin, A.V. Suvorov, H.F. Bettinger, H.F. Schaefer III, J. Am. Chem. Soc. 121 (1999) 5687–5699.
[39] A. Boutalib, J. Mol. Struct. (Theochem) 623 (2003) 121–126.
[40] F. Jensen, Introduction to Computational Chemistry, Wiley, New York, NY, 1999, pp. 172, 173, 217–234.
[41] T. Clark, A Handbook of Computational Chemistry, Wiley, New York, NY, 1985, pp. 289–291.
[42] S.F. Boys, F. Bernardi, Mol. Phys. 19 (1970) 553–566.
[43] M.J. Frisch, J.E. Del Bene, J.S. Binkley, H.F. Schaefer III, J. Chem. Phys. 84 (1986) 2279–2289.
[44] T.E. Mallouk, G.L. Rosenthal, G. Müller, R. Brusasco, N. Bartlett, Inorg. Chem. 23 (1984) 3167–3173.
[45] K.O. Christe, D.A. Dixon, D. McLemore, W.W. Wilson, J.A. Sheehy, J.A. Boatz, J. Fluorine Chem. 101 (2000) 151–153.
[46] R. Cipollini, F. Grandinetti, J. Chem. Soc., Chem. Commun. 7 (1995) 773–774.
[47] A. Cunje, V.I. Baranov, Y. Ling, A.C. Hopkinson, D.K. Bohme, J. Phys. Chem. A 105 (2001) 11073–11079.
[48] A.E. Ketvirtis, V.I. Baranov, Y. Ling, A.C. Hopkinson, D.K. Bohme, Int. J. Mass Spectrom. 185–187 (1999) 381–392.
[49] S.S. Yang, P. Wong, S. Ma, R.G. Cooks, J. Am. Soc. Mass Spectrom. 7 (1996) 198–204.
[50] V. Branchadell, A. Oliva, J. Mol. Struct. (Theochem) 236 (1991) 75–84.
[51] K. Aarset, Q. Shen, H. Thomassen, A.D. Richardson, K. Hedberg, J. Phys. Chem. A 103 (1999) 1644–1652.
[52] M.E. Jacox, K.K. Irikura, W.E. Thompson, J. Chem. Phys. 103 (1995) 5308–5314.
[53] D. Forney, M.E. Jacox, K.K. Irikura, J. Chem. Phys. 101 (1994) 8290–8295.
[54] I. Krossing, I. Raabe, J. Am. Chem. Soc. 126 (2004) 7571–7577.
[55] A. Beste, O. Krämer, A. Gerhard, G. Frenking, Eur. J. Inorg. Chem. (1999) 2037–2045.
[56] G.A. Olah, G. Rasul, L. Heiliger, G.K.S. Prakash, J. Am. Chem. Soc. 118 (1996) 3580–3583.
[57] V. Branchadell, A. Sbai, A. Olivia, J. Phys. Chem. 99 (1995) 6472–6476.
[58] S. Dapprich, G. Frenking, J. Phys. Chem. 99 (1995) 9352–9362.
[59] D.C. Young, Computational Chemistry, Wiley, New York, NY, 2001, pp. 99–106.
[60] R.S. Mulliken, J. Chem. Phys. 23 (1955) 1833–1840.
[61] (a) A.E. Reed, R.B. Weinstock, F. Weinhold, J. Chem. Phys. 83 (1985) 735–746;
(b) A.E. Reed, L.A. Curtiss, F. Weinhold, Chem. Rev. 88 (1988) 899–926;
(c) E.D. Glendening, J.K. Badenhoop, A.E. Reed, J.E. Carpenter, C.M. Bohmann, C.M. Morales, F. Weinhold, NBO Version 5. 0, Theoretical Chemistry Institute, University of Wisconsin, Madison, 2001.
[62] E.D. Jemmis, K.T. Giju, J. Leszczynski, J. Phys. Chem. A 101 (1997) 7389–7395.
[63] (a) E.D. Glendening, F. Weinhold, J. Comput. Chem. 19 (1998) 593–609;
(b) E.D. Glendening, F. Weinhold, J. Comput. Chem. 19 (1998) 610–627;
(c) E.D. Glendening, J.K. Badenhoop, F. Weinhold, J. Comput. Chem. 19 (1998) 628–646.
[64] L. Pauling, The Nature of the Chemical Bond, 3rd ed. Cornell University Press, Ithaca, NY, 1960, p. 260.
[65] A. Bondi, J. Phys. Chem. 68 (1964) 441–451.
[66] (a) D. Ohlmann, C.M. Marchand, H. Grützmacher, G.S. Chen, D. Farmer, R. Glaser, A. Currao, R. Nesper, H. Pritzkow, Angew. Chem. Int. Ed. Engl. 35 (1996) 300–303;
(b) H. Grützmacher, C.M. Marchand, Coord. Chem. Rev. 163 (1997) 287–344.
[67] A.D. Becke, K.E. Edgecombe, J. Chem. Phys. 92 (1990) 5397–5403.
[68] B. Silvi, A. Savin, Nature 371 (1994) 683–686.
[69] A. Savin, B. Silvi, F. Colonna, Can. J. Chem. 74 (1996) 1088–1096.
[70] D.B. Chesnut, Chem. Phys. 271 (2001) 9–16.
[71] A.L. Allred, E.G. Rochow, J. Inorg. Nucl. Chem. 5 (1958) 264–268, the quoted group 17 electronegativity values are: F (4.10), Cl (2.83), Br (2.74), I (2.21).
[72] M.J. Frisch, G.W. Trucks, H.B. Schlegel, G.E. Scuseria, M.A. Robb, J.R. Cheeseman, V.G. Zakrzewski, J.A.J. Montgomery, R.E. Stratmann, J.C. Burant, S. Dapprich, J.M. Millam, A.D. Daniels, K.N. Kudin, M.C. Strain, O. Farkas, J. Tomasi, V. Barone, M. Cossi, R. Cammi, B. Mennucci, C. Pomelli, C. Adamo, S. Clifford, J. Ochterski, G.A. Petersson, P.Y. Ayala, Q. Cui, K. Morokuma, P. Salvador, J.J. Dannenberg, D.K. Malick, A.D. Rabuck, K. Raghavachari, J.B. Foresman, J. Cioslowski, J.V. Ortiz, A.G. Baboul, B.B. Stefanov, G. Liu, A. Liashenko, P. Piskorz, I. Komaromi, R. Gomperts, R.L. Martin, D.J. Fox, T. Keith, M.A. Al-Laham, C.Y. Peng, A. Nanayakkara, M. Challacombe, P.M.W. Gill, B. Johnson, W. Chen, M.W. Wong, J.L.

Andres, C. Gonzalez, M. Head-Gordon, E.S. Replogle, J.A. Pople, Gaussian 98 (Revision A.11), Gaussian Inc., Pittsburgh, PA, 2001.
[73] Basis sets were obtained from the Extensible Computational Chemistry Environment Basis Set Database, http://www.emsl.pnl.gov/forms/basisform.html..
[74] S. Noury, X. Krokidis, F. Fuster, B. Silvi, TopMod Package, Laboratoire de Chimie Théorique, University of Paris VI, Paris, 1998.
[75] (a) L. Laaksonen, J. Mol. Graph. 10 (1992) 33–34;
(b) D.L. Bergman, L. Laaksonen, A. Laaksonen, J. Mol. Graph. Model. 15 (1997) 300–306.